DOI: 10.1002/ejic.200701154

Syntheses, Structures and Magnetic Properties of New Chalcogen-Bridged Heterodimetallic Cluster Compounds with Heterocubane Structure

Bettina Bechlars,[a] Ibrahim Issac,[a] Robert Feuerhake,[b] Rodolphe Clérac,[c] Olaf Fuhr,[b] and Dieter Fenske*[a,b]

Keywords: Niobium / Tantalum / Transition metals / Clusters / Heterocubanes

The reaction of nickel, iron and cobalt complexes with MCl_5 (M = Nb, Ta) and silylated chalcogen compounds in the presence of phosphane ligands yield the cluster compounds $[Nb_2Ni_2S_4Cl_4(PPh_3)_2(CH_3CN)_2]$ (**1**), $[Nb_2Ni_2Se_4Cl_4(PPh_3)_2(CH_3CN)_2]$ (**2**), $[Ta_2Ni_2S_4Br_4(PPh_3)_2(CH_3CN)_2]$ (**3**), $[Ta_2Ni_2Se_4Br_4(PPh_3)_2(CH_3CN)_2]$ (**4**), $[Ni_3S_2(PMe_3)_6][Ta_3NiS_4(PMe_3)_4Cl_6]_2$ (**5**), $[Fe(dppm)_2(CH_3CN)_2][NbFe_3S_4Cl_3(dppm)(CH_3CN)]_2$ (**6**) [dppm = (diphenylphosphanyl)methane], $[Fe(dppm)_2(CH_3CN)_2][TaFe_3S_4Cl_3(dppm)(CH_3CN)]_2$ (**7**), $[FeCl(dppmSe)_2][TaFe_3Se_4Cl_3(dppm)(CH_3CN)]$ (**8**) and $[NbCo_3Se_4(PPh_3)_3(CH_3CN)_3][CoCl_3(PPh_3)]$ (**9**). The compounds $(Et_4N)_3[NbFe_2S_4(SPh)_4]$ (**10**) and $(Et_4N)_3[NbFe_2Se_4(SPh)_4]$ (**11**) were obtained by treating $(Et_4N)_2[Fe(SPh)_4]$ with Li_3NbE_4 (E = S, Se). $(Et_4N)_3[Nb_2Fe_6S_8(SPh)_9]$ (**12**) was synthesized by adding $FeCl_2$ to compound **10** used as starting material. $(Et_4N)_3[Nb_2Fe_6Se_8(SePh)_9]$ (**13**) (which is isostructural to **12**) was synthesized by treating $FeCl_2$ with NaSe*t*Bu, $NbCl_5$ and $PhSeSiMe_3$.

Introduction

Transition metal chalcogenide cluster compounds with a heterocubane core represent a unique area of cluster chemistry. The interest in this class of compounds stems from their use as potential models for different catalytic processes with industrial and biological applications[1–4] as well as their use as optical limiters and X-ray contrast agents.[5–8]

The first cubane-like cluster was found in the redox-active unit of the electron-transfer protein ferredoxin and features an $[Fe_4S_4]$ core. Other important metalloenzymes such as the iron-molybdenum cofactor of nitrogenase contain heteronuclear transition metal clusters. Much effort was put into the synthesis of compounds that are capable of mimicking these active centres, and the discovery of vanadium as part of a heterodimetallic cluster in nitrogenase[9] led to an increasing interest in examining heterocubanes containing group 5 transition metals.[10,11] Thus, a number of compounds are known with an $[M_{4-x}M'_xE_4]$ cluster core containing M = Mo, W, V; M′ = Fe, Cu and E = S, such as the compounds $(Me_4N)[VFe_3S_4Cl_3(dmf)_3]$, $(Me_4N)[MoFe_3S_4(LS_3)(Cl_4\text{-cat})(dmf)]$ (LS_3 = trithiol ligand, Cl_4-cat = tetrachlorocatecholate),[12] and $(Et_4N)_3[W_2Fe_6S_8(SPh)_6(OMe)_3]$,[13] that contain single heterocubanes and the compounds $(Bu_4N)_4[(Cl_4\text{-cat})(n\text{Pr}_3\text{P})MoFe_3S_4(BH_4)_2]$[14] and $(Et_4N)_3[\{Cl_4\text{-cat})(n\text{Pr}_3\text{P})MoFe_3S_4Cl\}_3(\mu\text{-}SCH_2Ph)_3]$[15] with double or triply bridged heterocubanes, respectively, whereas only a few candidates were synthesized featuring the same cluster motif with M = Nb, Ta, M′ = Fe, Co, Ni, Cu and E = S, Se, for example $[Ta_2Ni_2E_4Cl_4(PPh_3)_2(CH_3CN)_2]$ (E = S, Se), $[TaCo_3S_4(NCS)_3(Pt\text{Bu}_3)_3]$,[16] and $(Et_4N)_3[Nb_2Fe_6S_8(SEt)_9]$.[17] In continuation of earlier work,[11,16] we want to present here syntheses and structure determinations (in the figures all hydrogen atoms are omitted for clarity) of new heterocubane-like compounds containing either niobium or tantalum combined with the electron-rich transition metals iron, cobalt or nickel, as well as the results of magnetic measurements performed on selected examples of these clusters.

Results and Discussion

Most of the structures that are described in this report contain a heterocubane $[M_nM'_{4-n}E_4]$ cluster core (M = Nb or Ta; M′ = Fe, Co, or Ni; E = S, Se). All the heterocubane structures have very similar features. The μ_3-bridging chalcogenido ligands usually carry a negative charge of –2 and possess one lone pair, whereas the metal atoms can adopt different positive oxidation states. Therefore, the chalcogen ions have a larger radius than the metal ions and need more space which leads to the following distortion of the heterocubane compared to a cube: The angles at the metal atoms tend to be larger, and the angles at the chalcogen atoms tend to be smaller than 90°. We will not explicitly mention this when we describe the structures, but we will point out

[a] Institut für Anorganische Chemie, Universität Karlsruhe, Engesserstr. 15, 76133 Karlsruhe, Germany
[b] Institut für Nanotechnologie, Forschungszentrum Karlsruhe, Hermann-von-Helmholtz-Platz 1, 76344 Eggenstein-Leopoldshafen, Germany
[c] Université Bordeaux 1, CNRS, Centre de Recherche Paul Pascal (UPR-CNRS 8641), 115, Avenue du Dr. A. Schweitzer, 33600 Pessac, France

exceptions. The values for these angles are given in Table 1. The M_4 (M = metal atom) tetrahedral subunit inscribed into the metal chalcogenide cubes is more or less distorted. The deltahedral angles and the M–M distances within this M_4 tetrahedron are used to describe the degree of this distortion.

Table 1. Angles [°] within in the heterocubane cores.

Compound	M–E–M	E–M–E
1	66.23(4)–73.72(4)[1]	100.80(4)–112.99(5)[a]
2	63.62(3)–70.65(3)[2]	102.46(4)–116.26(5)[b]
3	66.19(7)–73.94(6)[3]	101.24(8)–111.54(9)[c]
4	63.15(5)–70.50(4)	103.14(4)–115.00(5)[d]
5	70.84(10)–97.43(13)	87.90(11)–113.32(10)
6	71.4(2)–73.9(2)	102.5(2)–108.4(2)
7	69.90(10)–74.29(11)	103.08(13)–108.43(11)
8	64.95(7)–70.77(6)	104.99(3)–107.07(4)
9	66.71(4)–70.17(5)	102.59(4)–118.47(6)
12	72.87(4)–73.88(2)	101.02(2)–108.16(4)
13	69.92(3)–70.82(3)	103.33(2)–110.61(4)

[a] The angles within the [Nb1–S3–Nb2–S4] ring [86.52(4)–89.44(4)°] are not included. [b] The angles within the [Nb1–Se3–Nb2–Se4] ring [87.03(3)–88.56(3)°] are not included. [c] The angles within the [Ta1–S3–Ta2–S4] ring [87.49(7)–88.62(7)°] are not included. [d] The angles within the [Ta1–Se3–Ta2–Se4] ring [85.85(4)–90.06(4)°] are not included.

Table 2 provides an overview of these values for the discussed structures. In all of the following compounds that contain a heterocubane cluster core, the early transition metal atoms (Nb or Ta) are found within a more or less distorted octahedral ligand environment, and the late transition metal atoms (Fe, Co, or Ni) are placed in a more or less distorted tetrahedral coordination sphere. The associated angles are grouped together in Table 3 and will not be discussed in detail. Each of the polyhedra surrounding a metal atom share a common E_2 edge with two neighbouring polyhedra and a common face with the tetrahedral E_4 subunit of the heterocubane. The crystallographic data for all presented compounds are given in Tables 4 and 5.

The oxidation states of the metal atoms are determined by assuming that the chalcogen atoms adopt the oxidation state –II. It is not always possible to tell the oxidation states and numbers of unpaired electrons located at the metal atoms because there is usually more than one meaningful answer. In some cases, presuming an electron-delocalized cluster core is even more reasonable. We supported the assignments of oxidation states and assumptions for the electron distribution within the cluster core with magnetic measurements where possible.

Analogously to previously published syntheses[16] the reactions shown in Scheme 1 afforded the compounds $[Nb_2Ni_2S_4Cl_4(PPh_3)_2(CH_3CN)_2]\cdot 2CH_3CN$ (**1**·$2CH_3CN$), $[Nb_2Ni_2Se_4Cl_4(PPh_3)_2(CH_3CN)_2]\cdot 2CH_3CN$ (**2**·$2CH_3CN$), $[Ta_2Ni_2S_4Br_4(PPh_3)_2(CH_3CN)_2]\cdot 2.5CH_3CN$ (**3**·$2.5CH_3CN$), and $[Ta_2Ni_2Se_4Br_4(PPh_3)_2(CH_3CN)_2]\cdot 2.5CH_3CN$ (**4**·$2.5CH_3CN$). The cluster molecules are structurally similar to the known clusters $[Ta_2Ni_2E_4Cl_4(PPh_3)_2(CH_3CN)_2]$ (E = S, Se)[16] and $[Ta_2Cu_2S_4Cl_4(PPh_3)_2(CH_3CN)_2]$.[20] The molecular structure of **1** is illustrated in Figure 1 as a representative molecular unit of **1**–**4**.

The heterocubane consists of two niobium (**1**, **2**) or two tantalum (**3**, **4**), two nickel and four chalcogen atoms. Except for the angles within the [Nb(1)–E(3)–Nb(2)–E(4)] (**1**, **2**) and [Ta(1)–E(3)–Ta(2)–E(4)] (**3**, **4**) rings that are very

Table 2. Distances [pm] and angles [°] in the M_4 tetrahedron.

Compound	M–M–M	M–M	M–M′	M′–M′
1	50.91(1)–77.72(2)	342.1(1)	271.7(1)–274.7(1)	242.5(1)
2	50.34(2)–79.18(3)	353.0(1)	276.7(1)–279.4(1)	246.0(1)
3	51.61(1)–76.41(3)	338.2(1)	272.7(1)–275.1(1)	243.1(2)
4	50.97(1)–77.74(3)	348.0(1)	276.6(1)–278.8(1)	245.7(2)
5	48.01(1)–83.99(8)	358.9(1)	268.2(2)–270.7(2)	–
6	58.78(9)–60.94(9)	–	273.5(4)–276.7(4)	268.8(5)–273.3(5)
7	58.38(6)–61.16(6)	–	271.5(2)–276.9(2)	265.2(2)–273.6(2)
8	56.28(6)–61.86(3)	–	277.0(1)–282.4(2)	262.0(3)–277.7(2)
9	58.23(4)–60.93(4)	–	269.1(2)–269.6(2)	261(2)–263.9(2)
12	57.93(2)–61.04(1)	–	279.0(1)	270.2(1)
13	58.14(3)–60.93(1)	–	282.7(1)	274.7(1)

Table 3. Angles [°] within the coordination sphere of the metal atoms.

Compound	L–M–L	L–M′–L
1	80.60(11)–100.99(4) and 164.85(4)–174.99(10)	104.04(5)–114.08 (5)
2	80.72(13)–103.38(3) and 162.95(4)–172.13(13)	102.34(5)–115.26(5)
3	79.80(2)–101.81(8) and 163.82(6)–173.60(2)	104.75(9)–114.68(9)
4	79.2(2)–103.55(4) and 162.51 (4)–171.9(2)	102.74(9)–115.00(5)
5	77.99(15)–102.34(17) and 161.07(15)–176.30(16)	105.28(12) and 113.32(10)
6	62.77(17)–103.9(2) and 156.20(18)–159.14(19)	102.5(2)–119.2(3)
7	63.19(8)–104.59(9) and 155.47(9)–158.6(2)	103.08(13)–118.53(13)
8	63.19(10)–107.07(4) and 154.27(6)–162.2(3)	105.22(6)–117.46(15)
9	79.4(3)–103.57(4) and 161.2(2)–165.10(19)	104.90(6)–118.47(6)]
12	71.24(2)–101.02(2) and 158.52(2)	100.22(3)–119.76(4)
13	70.95(2)–95.14(2) and 156.25(3)	97.43(3)–119.22(4)

Table 4. Crystallographic data for **1**–**6**: Data were obtained with a STOE IPDS diffractometer using graphite-monochromated Mo-K_α radiation (λ = 0.71073 Å). The structures were solved by direct methods and refined by full-matrix least squares on F^2 (all data) using the SHELXTL software package.[18] Hydrogen atoms were placed in calculated positions, non-hydrogen atoms were assigned anisotropic thermal parameters.[a]

	1·2CH_3CN	**2**·2CH_3CN	**3**·2.5CH_3CN
Empirical formula	$C_{40}H_{36}Cl_4N_2Nb_2Ni_2P_2S_4$	$C_{40}H_{36}Cl_4N_4Nb_2Ni_2P_2Se_4$	$C_{40}H_{36}Br_4N_2Ni_2P_2S_4Ta_2$
Formula mass [g/mol]	1179.95	1367.53	1533.84
Temperature [K]	173(2)	100(2)	200(2)
Crystal system	monoclinic	triclinic	monoclinic
Space group	*C*2/*c*	$P\bar{1}$	*C*2/*c*
Unit-cell dimensions			
a [Å]	36.797(7)	12.275(3)	37.371(8)
b [Å]	10.740(2)	14.693(3)	10.918(2)
c [Å]	26.090(5)	16.275(3)	25.963(5)
α [°]	90	83.40(3)	90
β [°]	96.41(3)	82.35(3)	96.05(3)
γ [°]	90	76.17(3)	90
V [Å^3]	10246(4)	2814(1)	10534(4)
Z	8	2	8
Density (calcd.) [g cm^{-3}]	1.636	1.711	2.064
Absorption coefficient [mm^{-1}]	1.630	3.922	8.135
F(000)	5072	1412	6248
θ range of data collection [°]	3.66–31.92	1.72–27.03	3.34–31.93
Reflexions collected	22105	15707	41018
Independent reflexions	11102 (R_{int} = 0.0436)	10757 (R_{int} = 0.0378)	11958 (R_{int} = 0.1270)
Number of refined parameters	562	538	579
Final *R* indices	R_1 = 0.0497, wR_2 = 0.1720	R_1 = 0.0579, wR_2 = 0.1788	R_1 = 0.0759, wR_2 = 0.2239
Max./min. residual electron density [A^{-3}]	1.944/–1.715	1.972/–1.870	5.430/–6.326
$\|E^2 - 1\|$	1.019	0.992	0.999
GooF	1.100	1.032	1.091
Flack parameter	–	–	–
	4·2.5CH_3CN	**5**	**6**·4CH_3CN·2CH_2Cl_2
Empirical formula	$C_{40}H_{36}Br_4N_2Ni_2P_2Se_4Ta_2$	$C_{42}H_{126}Cl_{12}Ni_5P_{14}S_{10}Ta_6$	$C_{108}H_{100}Cl_6Fe_7N_4Nb_2P_8S_8$
Formula mass [g/mol]	1721.45	3190.26	2747.79
Temperature [K]	150(2)	197(2)	150(2)
Crystal system	monoclinic	trigonal	monoclinic
Space group	*C*2/*c*	*P*31*c*	$P2_1/n$
Unit cell dimensions			
a [Å]	37.477(8)	17.106(2)	25.279(5)
b [Å]	10.915(2)	17.106(2)	14.967(3)
c [Å]	26.049(5)	20.487(4)	38.693(8)
α [°]	90	90	90
β [°]	95.86(3)	90	106.61(3)
γ [°]	90	120	90
V [Å^3]	10600(4)	5191(2)	14029(5)
Z	8	2	4
Density (calcd.) [g cm^{-3}]	2.235	2.041	1.459
Absorption coefficient [mm^{-1}]	10.671	7.928	7.940
F(000)	6648	3060	6248
θ range of data collection [°]	1.82 to 27.17	3.77 to 31.86	1.60 to 17.89
Reflexions collected	41347	19618	26083
Independent reflexions	11599 (R_{int} = 0.1651)	8276 (R_{int} = 0.0902)	9363 (R_{int} = 0.1181)
Number of refined parameters	527	268	1403
Final *R* indices	$R1$ = 0.0809, $wR2$ = 0.2455	R_1 = 0.0764, wR_2 = 0.2115	R_1 = 0.0982, wR_2 = 0.2841
Max./min. residual electron density [A^{-3}]	5.416/–5.627	4.571/–4.791	2.463/–0.986
$\|E^2 - 1\|$	1.001	0.812	0.967
GooF	1.242	1.100	1.044
Flack parameter	–	–0.024(14)	

[a] CCDC-658747, -658748, -658749, -658750, -658751, and -658752 contain the supplementary crystallographic data for this paper. These data can be obtained free of charge from The Cambridge Crystallographic Data Centre via www.ccdc.cam.ac.uk/data_request/cif.

close to 90°, the heterocubane is distorted as expected (see Table 1). The angles and distances within the Nb_2Ni_2 (**1**, **2**) and Ta_2Ni_2 (**3**, **4**) tetrahedral subunits strongly deviate from the ideal values (see Table 2). In **1**–**4** the niobium and tantalum atoms are each coordinated by one acetonitrile, three μ_3-chalcogenido and two halido ligands in a distorted octa-

Table 5. Crystallographic data for **7**–**13**. Data were obtained with a STOE IPDS diffractometer using graphite-monochromated Mo-K_α radiation (λ = 0.71073 Å). The structures were solved by direct methods and refined by full-matrix least squares on F^2 (all data) using the SHELXTL software package.[19] Hydrogen atoms were placed in calculated positions, non-hydrogen atoms were assigned anisotropic thermal parameters.[a]

	7·4CH_3CN·2CH_2Cl_2	**8**·CH_2Cl_2	**9**·4CH_3CN	**10**
Empirical formula	$C_{108}H_{100}Cl_6Fe_7N_4P_8S_8Ta_2$	$C_{78}H_{69}Cl_4Fe_4NP_6Se_6Ta$	$C_{78}H_{69}Cl_3Co_4N_3NbP_4Se_4$	$C_{48}H_{80}Fe_2N_3NbS_8$
Formula mass [g/mol]	2923.87	2226.16	1923.16	1160.24
Temperature [K]	173(2)	110(2)	110(2)	150(2)
Crystal system	monoclinic	orthorhombic	triclinic	monoclinic
Space group	$P2_1/n$	$Pbcm$	$P\bar{1}$	$C2/c$
Unit cell dimensions				
a [Å]	25.868(5)	13.251(3)	13.866(3)	27.487(6)
b [Å]	14.959(3)	18.781(4)	15.455(3)	11.049(2)
c [Å]	38.805(8)	33.217(7)	21.677(4)	20.565(4)
α [°]	90	90	101.49(3)	90
β [°]	105.96(3)	90	94.15(3)	117.53(3)
γ [°]	90	90	102.83(3)	90
V [Å^3]	14437(5)	8267(3)	4405(2)	5538(2)
Z	4	4	2	4
Density (calcd.) [g cm^{-3}]	1.497	1.846	1.574	1.391
Absorption coefficient [mm^{-1}]	2.625	4.999	2.727	1.056
F(000)	6484	4468	2084	2440
2θ range of data collection [°]	3.24–31.91	1.54–27.12	1.50–28.28	3.08–31.80
Reflexions collected	112730	51804	39157	22144
Independent reflexions	34552 (R_{int} = 0.0894)	9260 (R_{int} = 0.2403)	20044 (R_{int} = 0.1010)	6374 (R_{int} = 0.0430)
Number of refined parameters	1398	429	954	325
Final R indices	R_1 = 0.0973; wR_2 = 0.2893	R_1 = 0.0680; wR_2 = 0.1954	R_1 = 0.0737; wR_2 = 0.1540	R_1 = 0.0540, wR_2 = 0.1678
Max./min. residual electron density [A^{-3}]	4.006/–4.056	1.735/–2.151	0.878/–1.448	1.534/–1.389
$\|E^2 - 1\|$	0.972	0.993	0.854	0.981
GooF	1.073	0.960	1.048	1.107

	11	**12**·CH_3CN	**13**·CH_3CN
Empirical formula	$C_{48}H_{80}Fe_2N_3NbS_4Se_4$	$C_{78}H_{105}Fe_6N_3Nb_2S_{17}$	$C_{78}H_{105}Fe_6N_3Nb_2Se_{17}$
Formula mass [g/mol]	1347.84	2150.73	2947.93
Temperature [K]	100(2)	150(2)	150(2)
Crystal system	monoclinic	hexagonal	hexagonal
Space group	$C2/c$	$P6_3/m$	$P6_3/m$
Unit cell dimensions			
a [Å]	27.780(6)	17.804(3)	18.150(3)
b [Å]	11.193(2)	17.804(3)	18.150(3)
c [Å]	20.663(4)	16.712(3)	16.907(3)
α [°]	90	90	90
β [°]	117.83(3)	90	90
γ [°]	90	120	120
V [Å^3]	5682(2)	4588(1)	4824(2)
Z	4	2	2
Density (calcd.) [g cm^{-3}]	1.576	1.584	2.056
Absorption coefficient [mm^{-1}]	3.445	1.592	7.560
F(000)	2728	2245	2858
2θ range of data collection [°]	1.66–27.08	3.34–31.86	3.43–31.73
Reflexions collected	12458	36953	39113
Independent reflexions	5766 (R_{int} = 0.1259)	4594 (R_{int} = 0.0499)	4635 (R_{int} = 0.1043)
Number of refined parameters	323	210	198
Final R indices	R_1 = 0.0766, wR_2 = 0.2168	R_1 = 0.0495; wR_2 = 0.1522	R_1 = 0.0550; wR_2 = 0.1639
Max./min. residual electron density [A^{-3}]	1.831/–1.011	3.573/–1.648	3.414/–2.103
$\|E^2 - 1\|$	0.931	1.025	1.016
GooF	0.973	1.251	1.154

[a] CCDC-658753, -658754, -658755, -658756, -658757, -658758 and -658759 contain the supplementary crystallographic data for this paper. These data can be obtained free of charge from The Cambridge Crystallographic Data Centre via www.ccdc.cam.ac.uk/data_request/cif.

hedral geometry (see Table 3). One triphenylphosphane and three μ_3-chalcogenido ligands surround the nickel atoms in a slightly distorted tetrahedral arrangement (see Table 3).

There are two possibilities to assign the oxidation states of the metal atoms in **1**–**4**. If the niobium and tantalum atoms, respectively, adopt the oxidation state +V (d^0), the

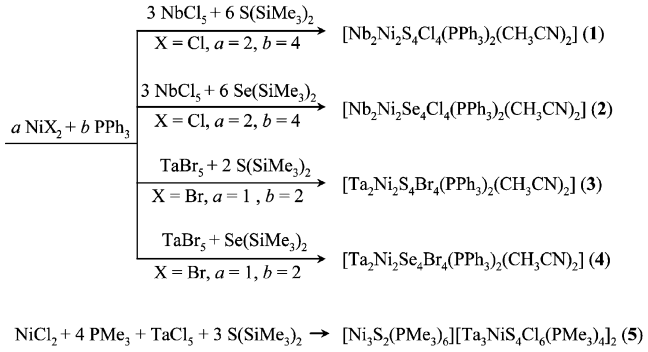

Scheme 1. Syntheses of **1**–**5**.

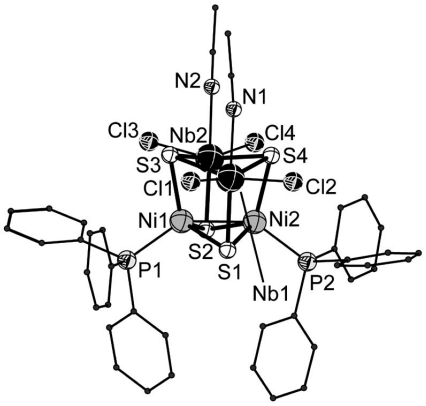

Figure 1. Molecular structure of **1** in the solid state. Selected bond lengths [pm]: **1**: Nb–S 236.4(1)–244.7(1), Nb–N 232.0(4)/233.6(4), Nb–Cl 240.3(1)–241.5(1), Ni–S 220.2(1)–224.1(1), Ni–P 219.0(1)/220.0(1); **2**: Nb–Se 249.1(1)–257.9(1), Nb–N 232.1(5)/235.2(5), Nb–Cl 242.6(2)–243.4(2), Ni–Se 232.7(1)–235.4(1), Ni–P 219.5(2)/220.6(2); **3**: Ta–S 234.3(2)–244.0(2), Ta–N 228.9(7)/230.0(8), Ta–Br 255.6(1)–257.6(1), Ni–S 221.6(2)–224.4(2), Ni–P 219.8(2)/220.7(2); **4**: Ta–Se 247.8(1)–256.5(1), Ta–N 226.5(7)/228.0(9), Ta–Br 256.3(1)–258.1(1), Ni–Se 233.3(2)–236.7(2), Ni–P 220.3(3)/221.0(3).

oxidation state +I has to be assigned to the nickel atoms (d^9). Without metal–metal bonds this would result in two unpaired electrons per cluster molecule. On the other hand if one assumes the oxidation state +IV (d^1) for the niobium and tantalum atoms, the nickel atoms have to adopt the oxidation state +II (d^8). Without metal–metal bonds this would lead to six unpaired electrons per cluster molecule. Up to now, we have not succeeded in isolating **1**, **2**, and **4** as sufficiently pure compounds for meaningful magnetic measurements. First experiments, however, reveal that the measured samples are weakly paramagnetic with susceptibilities much lower than the expected value for one unpaired electron per cluster molecule. This actually gives rise to the assumption that the cluster compound itself is diamagnetic and the sample contaminated with paramagnetic impurities. Compound **3**, however, can be isolated as a very clean product, and magnetic measurements reveal its diamagnetic nature as found for isostructural compounds, namely $[Ta_2Ni_2E_4Cl_4(PPh_3)_2(CH_3CN)_2]$ (E = S, Se).[16] This diamagnetic behaviour can be conclusively explained by tantalum atoms adopting the oxidation state +V (d^0), and the nickel atoms being in an oxidation state +I (d^9) with a single bond between the two nickel atoms. The observed Ni–Ni distances of 242.5(1) pm in **1**, 246.0(1) pm in **2**, 243.1(2) pm in **3**, and 245.7(2) pm in **4** are within the range of Ni–Ni bonds in known compounds such as $[Ni_2(\mu\text{-}t\text{Bu}_2\text{As})_2(PMe_3)_2]$[21] (242.9 pm), $[Ni_2(\mu\text{-}t\text{Bu}_2\text{P})_2(PMe_3)(CO)_2]$[22] (244.6 pm), and $[Ta_2Ni_2S_4Cl_4(PPh_3)_2(CH_3CN)_2]$[16] (241.2 pm) with a similar bonding situation. Furthermore, compounds **1**–**4** show the same architecture as $[Ta_2Cu_2S_4Cl_4(PPh_3)_2(CH_3CN)_2]$,[19] which contains copper atoms in the oxidation state +I.

The reaction of $NiCl_2$ and $TaCl_5$ with PMe_3 followed by addition of $S(SiMe_3)_2$ as shown in Scheme 1 affords $[Ni_3S_2(PMe_3)_6][Ta_3NiS_4(PMe_3)_4Cl_6]_2$ (**5**). This ionic compound consists of a $[Ta_3NiS_4(PMe_3)_4Cl_6]^-$ anion (**5a**) and an $[Ni_3S_2(PMe_3)_6]^{2+}$ cation (**5b**) which are shown in Figure 2. Both molecules contain a C_3 axis running through two atoms (Ni1 and S2 in **5a** and S5 and S6 in **5b**).

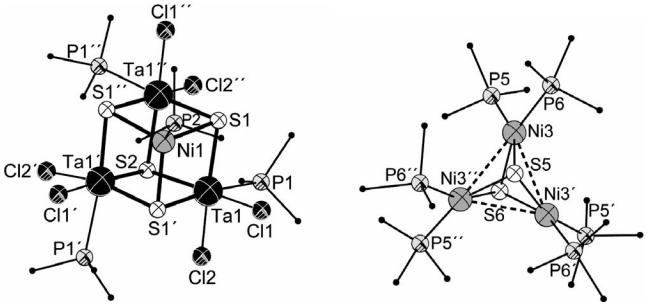

Figure 2. Molecular structures of **5a** (left) and **5b** (right) in the solid state. Selected bond lengths [pm]: **5a**: Ta1–S1 238.1(3), Ta1–S1′ 239.5(3), Ta1–Cl1 225.4(4), Ni1–S1 222.7(4), Ta1–S2 265.6(4), Ta1–P1 263.6(4), Ta1–Cl2 245.3(4), Ni1–P2 219.7(6); selected bond lengths [pm] and angles [°]: **5b**: Ni3–S5 218.1(5), Ni3–P5 217.5(5), Ni3–Ni3′ 182.9(3), Ni3–S6 216.9(5), Ni3–P6 218.5(5); S5–Ni3–S6 82.7(2), P5–Ni3–S6 91.5(2), P5–Ni3–P6 100.5(2), P5–Ni3–S5 160.65(17).

The heterocubane cluster core of **5a** is of the same type as the central heterocubane units of the cluster compounds $[Mo_3NiS_4(Cp)_3(AsPh_3)](CH_3C_6H_4SO_3)$,[23] $[Mo_3NiS_4(H_2O)_{10}](CH_3C_6H_4SO_3)_4$,[24] and $(Et_4N)[Ta_9Cu_{10}S_{24}Cl_8(PMe_3)_{14}]$,[19] because they are all formed by three early transition metal, one late transition metal and four sulfur atoms. The $[Ta_3NiS_4]$ unit of **5a** is significantly distorted. The angles within the three faces that contain the sulfur atom S2 are very close to 90° [85.00(14)–97.43(13)°], whereas the angles within the other three faces deviate from 90° in the typical manner [Ni1–S–Ta 70.84(10)° and S–Ni1–S 113.32(10)°]. The four metal atoms arrange in an almost perfect trigonal pyramid with the three tantalum atoms forming an equilateral triangle as the basis and the nickel atom forming the top of the pyramid (see Table 2). The tantalum atoms are octahedrally coordinated by three μ_3-sulfido, two terminal chlorido and one trimethylphosphane ligands in a distorted manner (see Table 3). Three μ_3-sulfido, and one trimethylphosphane ligand build a distorted tetrahedral coordination sphere around the nickel atoms (see Table 3).

Again there are several ways to describe the electron distribution among the metal atoms within **5a**. The oxidation states +IV (d^1) and +I (d^9) could be assigned to the tantalum and nickel atoms, respectively. Reducing the valence of one of the tantalum atoms by one (d^2) would lead to Ni^{II} (d^8). It is also possible that we are dealing with an electron-delocalized cluster core. The Ta–Ni distances are shorter than the sum of their covalence radii, but without any further information it is impossible to tell whether there are metal–metal bonds in this cluster. The structure of **5b** can be described as a trigonal bipyramid in which three nickel atoms occupy the equatorial and two sulfur atoms as μ_3-bridging ligands the axial positions. Besides the two μ_3-sulfido ligands, each of the three nickel atoms is coordinated by two trimethylphosphane ligands leading to a distorted square-planar coordination environment at the nickel atoms. The same architecture was found for the isoelectronic complexes $[Ni_3S_2(PEt_3)_6]^{2+}$[25] and $[Ni_3S_2(PPh_3)_4Cl_2]$.[26] Compound $[Ni_3S_2Cp_3]$[27] contains the trigonal-bipyramidal $[Ni_3S_2]$ unit. The Ni–Ni distances in **5b** [282.9(3) pm] are significantly shorter than in $[Ni_3S_2(PEt_3)_6]^{2+}$ [291.0(2) pm] and $[Ni_3S_2(PPh_3)_4Cl_2]$ [289.5(2)–293.4(2) pm], but comparable with the Ni–Ni distances in $[Ni_3S_2Cp_3]$ [280.1(5) pm]. In $[Ni_3S_2(PPh_3)_4Cl_2]$ and $[Ni_3S_2Cp_3]$ weak binding interactions are assumed. Furthermore, all these trinuclear nickel clusters contain 48 valence electrons which is the number of electrons needed for an electron-precise cluster with bonds along all of its triangle edges.

As shown in Scheme 2, $FeCl_2$ reacts with dppm, MCl_5 (M = Nb, Ta) and $S(SiMe_3)_2$ to afford the isostructural ionic compounds $[Fe(dppm)_2(CH_3CN)_2][NbFe_3S_4Cl_3(dppm)(CH_3CN)]_2 \cdot 4CH_3CN \cdot 2CH_2Cl_2$ (**6**·$4CH_3CN \cdot 2CH_2Cl_2$), and $[Fe(dppm)_2(CH_3CN)_2][TaFe_3S_4Cl_3(dppm)(CH_3CN)]_2 \cdot 4CH_3CN \cdot 2CH_2Cl_2$ (**7**·$4CH_3CN \cdot 2CH_2Cl_2$). $[Fe(Sedppm)_2Cl][TaFe_3Se_4Cl_3(dppm)(CH_3CN)] \cdot CH_2Cl_2$ (**8**·CH_2Cl_2), that differs from **6** and **7** mainly in the counter cation, can be obtained by the reaction of $[Fe_8Se_9(dppm)_3]$[28] with $TaCl_5$ (Scheme 2). The compounds are composed of $[MFe_3E_4Cl_3(dppm)(CH_3CN)]^-$ anions [M = Nb, E = S (**6a**); M = Ta, E = S (**7a**); M = Ta, E = Se (**8a**)] that show the same architecture as the anion in $(n-Pr_4N)[VFe_3S_4Cl_3(dppe)(CH_3CN)]$,[29] published by Holm et al., and are comparable to the anion $(Et_4N)_2[MoFe_3S_4Cl_3(mida)]$,[30] published by Coucouvanis et al., and $[Fe(dppm)_2(CH_3CN)_2]^{2+}$ (**6b** and **7b**) or $[Fe(Sedppm)_2Cl]^+$ cations (**8b**). The molecular structures of the anions **6a** and **8a** are shown in Figure 3.

The heterocubane cores of the anions are composed of one niobium or tantalum, three iron and four chalcogen atoms and are distorted in the typical manner (see Table 1). In these clusters, however, the deltahedral angles in the $[NbFe_3]$ and $[TaFe_3]$ tetrahedrons are very close to the ideal 60° and the metal–metal distances are within a narrow range (see Table 2). The niobium and tantalum atoms in **6a**, **7a**, and **8a** are each coordinated by three μ_3-sulfido, one bidentate dppm, and one acetonitrile ligand that form a distorted octahedral coordination sphere (see Table 3). Each of the iron atoms is surrounded by three μ_3-sulfido

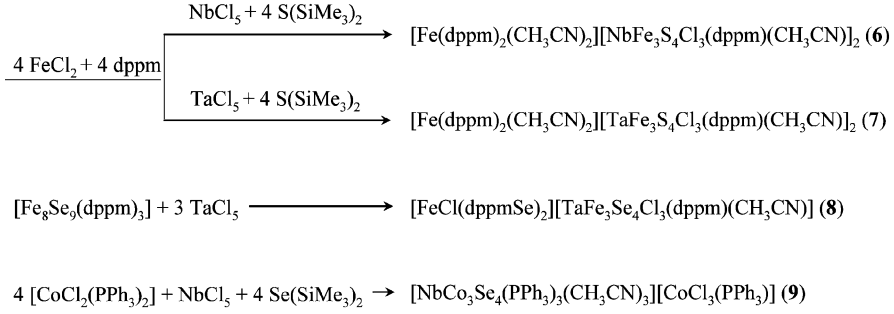

Scheme 2. Syntheses of **6**–**9**.

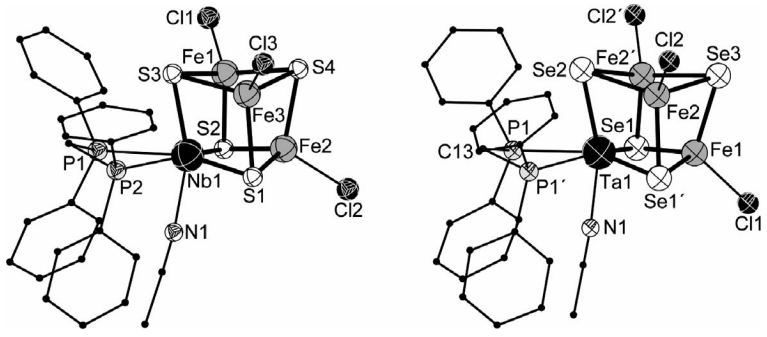

Figure 3. Molecular structures of the anions **6a** (left) and **8a** (right) in the solid state. Selected bond lengths [pm]: **6a**: Nb–S 236.5(5)–238.5(5), Nb–N 220.0(2), Nb–P 269.9(6)/271.2(6), Fe–S 227.8(6)–230.9(6), Fe–Cl 221.4(6); **7a**: Ta–S 237.0(2)–237.6(3), Ta–N 223.7(10), Ta–P 268.0(3)/270.5(3), Fe–S 228.5(3)–231.6(3), Fe–Cl 225.9(3); **8a**: Ta–Se 250.6(1)–252.1(2), Ta–N 224.4(1), Ta–P 270.1(2), Fe–Se 237.0(2)–245.5(1), Fe–Cl 221.0(4).

and one chlorido ligand that form a distorted tetrahedron (see Table 3).

Figure 4 (left) shows **6b**, which is a mononuclear Fe^{II} complex with an octahedral coordination sphere of two bidentate dppm ligands, and two acetonitrile molecules. Compound **8b**, also a mononuclear Fe^{II} complex, is shown in Figure 4 (right). The iron atom is coordinated by two Sedppm ligands through the selenium and one of the phosphorus atoms and one chlorido ligand in a distorted bipyramidal manner. The selenium and chlorine atoms occupy the equatorial and the phosphane atoms the axial positions. The Sedppm ligand has to be a result of a redox reaction taking place in the reaction mixture. The reaction mechanism should be similar to that described for $[MoFe_3S_4(Cl_4\text{-}cat)(PEt_3)(SPEt_3)_2Cl]$[31] where it is assumed that PEt_3 reductively desulfurizes $[MoFe_3S_4Cl_3(Cl_4\text{-}cat)(CH_3CN)]^{2-}$ leading to the formation of $SPEt_3$ by oxidizing P^{III} to P^{V}. We assume that the $[MFe_3S_4]^{2+}$ heterocubane cores (M = Nb, Ta) of **6a**–**8a** are not only comparable to the $[VFe_3S_4]^{2+}$ units examined by Holm et al.[28] and the $[MoFe_3S_4]^{3+}$ units examined by Coucouvanis et al.,[29] previously, but also show similarities in the electron distribution featuring electron-delocalized cluster cores. Holm et al. and Coucouvanis et al. found a ground state of $S = 3/2$ for their clusters and attributed an oxidation state of smaller than +IV to the vanadium and molybdenum atom and an oxidation state of larger than +II to the iron atoms. To verify a similar situation for **6a**, magnetic measurements were performed on **6** (Figure 5).

For the interpretation of these data, the cation **6b** can be ignored due to its diamagnetic nature. Indeed the Fe–P distances of **6b** [226.2(6)–229.4(3) pm] are comparable to those found in the very similar, diamagnetic cations of $[Fe(depe)_2(CH_3CN)_2](BF_4)_2$ [depe = bis(diethylphosphanyl)ethane][32] and $[Fe(odpdp)_2(CH_3CN)_2]I_2$ [odpdp = 1,2-bis(diphenylphosphanyl)benzene].[33] It is thus reasonable to assume a low-spin electron configuration for Fe^{II} in **6b**.

For temperatures higher than 80 K the product χT is equal to 3.65 cm^3K/mol {for two $[NbFe_3S_4Cl_3(dppm)(CH_3CN)]^-$ units} that corresponds well to a spin ground state of $S = 3/2$ for one cluster anion and is consistent with the spin ground state found for $[VFe_3S_4Cl_3]^-$. The experimental data can be fit to the Curie–Weiss law assuming that at low temperatures the cluster anions are antiferromagnetically coupled in the three-dimensional structure. This approximation – solid line in Figure 5 – leads to the values $g = 2.0$ and $\theta = -0.9$ K.

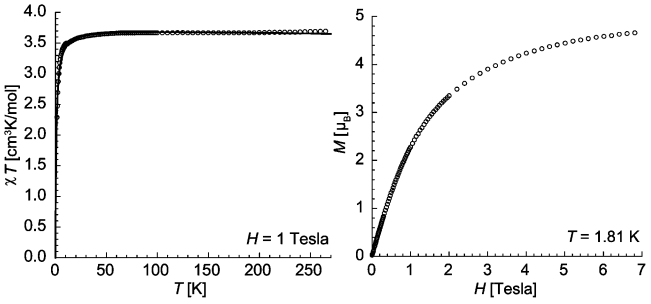

Figure 5. Magnetic measurements of **6**. Left: χT vs. T plot at 1 Tesla with the solid line being the best fit obtained using the Curie–Weiss law; right: M vs. H plot at 1.81 K.

The saturation value of the magnetisation for **6** is expected to be 6 μ_B considering that the magnetic moments of the cluster anions are all aligned in the field direction. At a field of 7 Tesla the magnetisation is found to be about 5 μ_B, and a saturation is not yet reached. The lack of saturation is probably coming from the combined effect of the intermolecular antiferromagnetic interactions and magnetic anisotropy.

A very similar behaviour can be observed for **8** (Figure 6). For temperatures between 30 and 200 K the product χT is roughly constant to 4.65 cm^3K/mol and decreases for temperatures lower than 30 K. For temperatures higher than 200 K a slight increase of χT can be observed and can be attributed to the thermal population of excited magnetic states.

As the trigonal-bipyramidally coordinated Fe^{II} in **8b** can adopt two possible electron configurations leading to $S = 0$ or $S = 2$[34] we can assume that **8a** has a spin ground state of $S = 3/2$ like $[VFe_3S_4Cl_3(dppm)(CH_3CN)]^-$, **6a** or $[TaFe_3S_4Br_4]^{2-}$. The experimental data below 70 K can be fit to a Curie–Weiss law with $C = 4.74$ cm^3K/mol and $\theta =$

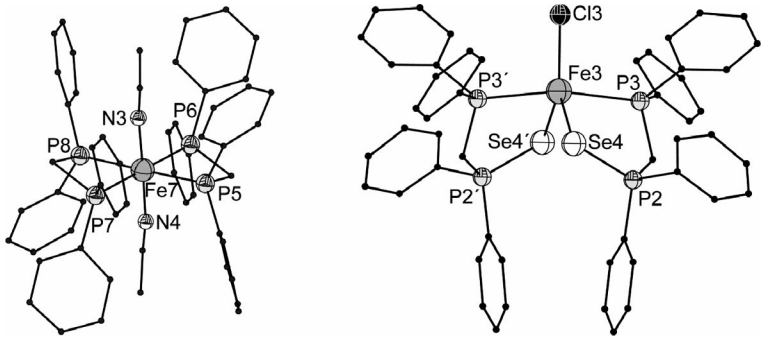

Figure 4. Molecular structures of the cations **6b** (left) and **8b** (right). Selected bond lengths [pm] and angles [°]: **6b**: Fe7–N3 196.0(2), Fe7–P 226.2(6)–228.8(6); N3–Fe7–N4 177.6(8), N–Fe7–P 87.0(5)–92.6(6), P5–Fe7–P6 73.1(2)–73.1(2), P5–Fe7–P7/P8 106.6(3)/178.9(3); **7b**: Fe7–N3 188.8(1), Fe7–P 226.6(3)–229.4(3), N3–Fe7–N4 178.8(4), N–Fe7–P 87.6(3)–93.3(3), P5–Fe7–P6 73.0(1), P5–Fe7–P7/P8 106.9(1)/178.9(1); **8b**: Fe3–Cl3 227.8(4), Fe3–Se4 256.5(2), Cl3–Fe3–Se4 126.92(4), P3–Fe3–P3′ 168.10(13), P3–Fe3–Cl3 95.95(7), Fe3–P3 252.0(3), Se4–Fe3–Se4′ 106.17(8), P3–Fe3–Se4 87.43(6).

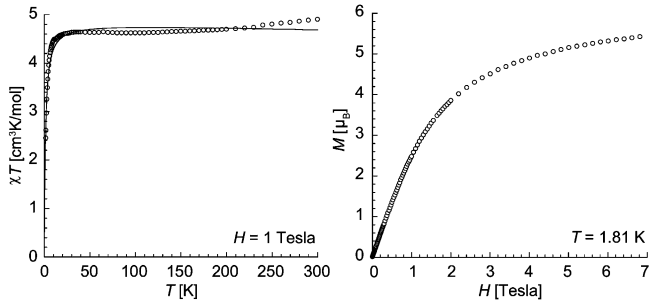

Figure 6. Magnetic measurements of **8**. Left: χT vs. T plot at 1 Tesla with the solid line being the best fit obtained using a Curie–Weiss law between 1.8 and 70 K; right: M vs. H plot at 1.81 K.

–1.0 K (solid line in Figure 6). On the basis of the result obtained for **6**, the contribution of the Curie constant from the anion **8a** should then be around 1.87 cm^3K/mol which induces the contribution of the cation **8b** to the Curie constant of about 2.9 cm^3K/mol. This value strongly suggest the presence of an $S = 2$ ground state for **8b**. This conclusion is further supported by the analysis of the bond lengths in **8b**. If the Fe–P_{ax} distances in the low-spin complex $[FeBr(pp_3)]^-$ {pp_3 = tris[2-(diphenylphosphanyl)ethyl]-phosphane} [221.4(3) pm][33] and in **8b** [252.0(3) pm] are compared, a significant difference can be seen that supports the assumption of a high-spin electron configuration of Fe^{II} in **8b** with four unpaired electrons. Considering the presence of $S = 3/2$ anion and $S = 2$ cation motifs in **8**, the saturation value of the magnetisation should be 7 μ_B. Experimental M vs. H data at 1.8 K are shown in Figure 6. At the highest available field (7 Tesla), the magnetisation is not saturated and reaches about 5.4 μ_B. As in **6**, the lack of saturation probably originates from the combined effect of the intermolecular antiferromagnetic interactions and magnetic anisotropy.

$[CoCl_2(PPh_3)_2]$ reacts with $NbCl_5$ and $Se(SiMe_3)_2$ as shown in Scheme 2 to afford the ionic compound $[NbCo_3Se_4(PPh_3)_3(CH_3CN)_3][CoCl_3(PPh_3)]\cdot 4CH_3CN$ (**9**·$4CH_3CN$). One formula unit of **9** contains an $[NbCo_3Se_4(PPh_3)_3(CH_3CN)_3]^+$ cation (**9a**) that is shown in Figure 7 and a $[CoCl_3(PPh_3)]^-$ anion.

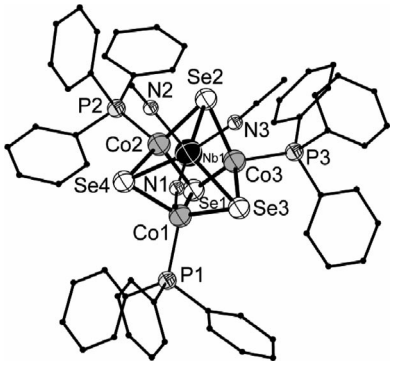

Figure 7. Molecular structure of **9a** in the solid state. Selected bond lengths [pm]: **9**: Nb1–Se 255.1(1)–255.7(1), Nb1–N 227.0(8)/231.1(7), Co–Se 229.3(2)–233.8(2), Co–P 219.2(2)–220.7(2).

The heterocubane cation represents the first structurally characterised molecular Nb–Co–Se compound and has a cluster core that is similar to the neutral tantalum compound $[TaCo_3S_4(PtBu_3)_3]\cdot PtBu_3\cdot 0.5CH_3CN$.[16] A number of compounds with an $[MM'_3S_4]$ heterocubane core are known that result from the coordination chemistry of tetrathiomolybdates {e.g. $(Et_4N)_2[MoFe_3S_4Cl_3(Cl_4\text{-cat})(L)]$[35] (R = Et, L = CH_3CN, $MeNH_2$, Cl_4-cat = tetrachlorocatecholate, $n = 2$, 3) or $(Et_4N)_2[MoFe_3S_4Cl_3(H_2cit)]$ (H_2cit = citrate dianion)[36] which serve as model compounds to mimic the coordinative environment of molybdenum in the iron-molybdenum cofactor of nitrogenases}. The heterocubane cluster core of **9a** is built up by one niobium, three cobalt, and four selenium atoms and is significantly distorted (see Table 1). The $[NbCo_3]$ tetrahedron, however, almost ideally represents a tetrahedron with deltahedral angles close to 60° and metal–metal distances falling into a small range (see Table 2). The niobium atom is coordinated by three μ_3-selenido ligands and three acetonitrile molecules that form a distorted $[Se_3N_3]$ octahedron (see Table 3) with each selenium atom being *cis*-coordinated to the other selenium atoms and *trans*-coordinated to one of the nitrogen atoms. The cobalt atoms are surrounded by three μ_3-selenido and one triphenylphosphane ligand forming a distorted tetrahedron (see Table 3). The oxidation state of the cobalt atom in the $[CoCl_3(PPh_3)]^-$ anion has to be +II. If each of the cobalt atoms in the cluster cation adopts the oxidation state +II (d^7), the oxidation state +III (d^2) has to be assigned to the niobium atom. It is also possible that the electrons are delocalized within the cluster core. All the Nb–Co distances are shorter than the sum of the covalent radii of the participating metal atoms [Nb–Co 269.1(2)–269.6(2) pm].

The reaction of $(Et_4N)_2[Fe(SPh)_4]$ with $Li_3NbS_4\cdot 2TMEDA$ (for **10**) and Li_3NbSe_4 (for **11**) yields the ionic compounds $(Et_4N)_3[NbFe_2S_4(SPh)_4]$ (**10**) and $(Et_4N)_3[NbFe_2Se_4(SPh)_4]$ (**11**) (Scheme 3). Compounds **10** and **11** consist of $[NbFe_2E_4(SPh)_4]^{3-}$ anions [E = S (**10a**), Se (**11a**)] and Et_4N^+ countercations. These two compounds are comparable to the known compounds $(Et_4N)_3[VFe_2S_4Cl_4]$ and $(Et_4N)_3[VFe_2S_4(SPh)_4]$[37] reported by Holm et al. The molecular structure of **10a** is represented in Figure 8.

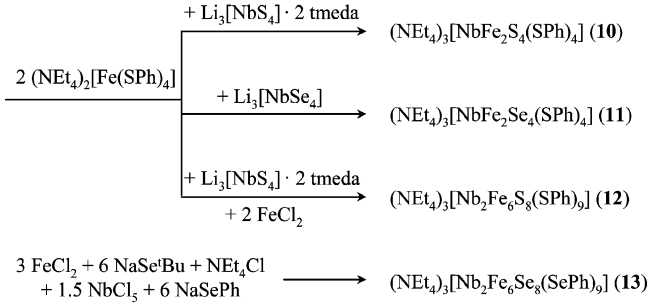

Scheme 3. Syntheses of **10**–**13**.

The $[NbE_4]^{3-}$ anion (E = S for **10**, Se for **11**) of the starting material acts as a bidentate ligand for each of the two iron atoms and replaces two phenylthiolate ligands of the

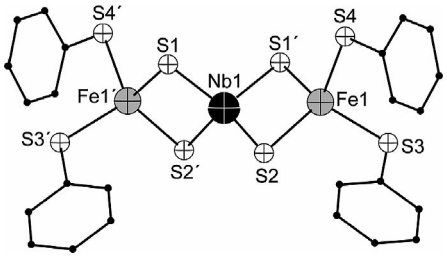

Figure 8. Molecular structure of **10a** in the solid state. Selected bond lengths [pm]: **10a**: Nb–Fe 282.1(1), Nb–S 228.8(1)/229.3(1), Fe–S_b 232.2(1)/232.9(1), Fe–S_t 231.3(1)/231.9(1); **11a**: Nb–Fe 288.7(1), Nb–Se 241.9(1)/241.6(2), Fe–Se_b 241.9(1)/244.3(2), Fe–Se_t 231.5(3)/231.9(3).

$[Fe(SPh)_4]^{2-}$ complex. This arrangement affords the formation of a trinuclear anion that contains a central $[NbE_4]$ unit [E = S (**10a**), Se (**11a**)] coordinated to two $Fe(SPh)_2$ units and leads to a distorted tetrahedral coordination sphere of all three metal atoms [E–Nb–E: **10a**: 105.50(3)–114.08(6)°; **11a**: 107.48(4)–113.45(7)°; E–Fe–E: **10a**: 97.77(4)–120.99(4)°; **11a**: 97.47(9)–120.81(10)°]. Assuming an oxidation state of +V (d^0) for the niobium atom, an oxidation state of +II (d^6) for the iron atoms with four unpaired electrons located at each iron atom, a spin ground state of $S = 2$ for each iron atom seems to be reasonable. To see if the magnetic moments at the iron atoms communicate with each other, magnetic measurements were performed on **10** which are shown in Figure 9.

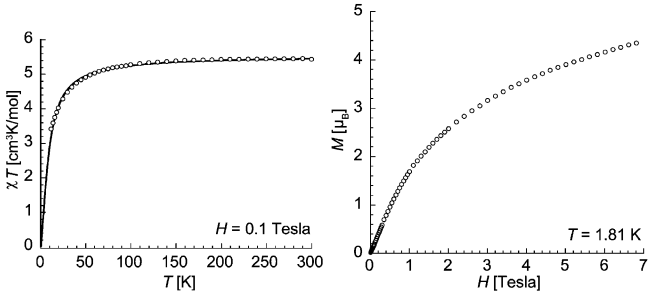

Figure 9. Magnetic measurements of **10**. Left: χT vs. T plot at 0.1 Tesla with the solid line being the best fit obtained using the Heisenberg $S = 2$ dimer model; right: M vs. H at plot at 1.81 K.

At temperatures higher than 100 K the product χT is about constant at 5.5 cm^3K/mol, close to the expected value (6 cm^3K/mol) for two isolated $S = 2$ magnetic moments. At low temperatures, χT decreases to reach 1.9 cm^3K/mol at 1.8 K. This feature can be interpreted considering the presence of antiferromagnetic coupling between the two iron spins through the bridging μ_2-chalcogenido ligands and the diamagnetic niobium ion. The experimental data of **10** have been fitted to an isotropic Heisenberg $S = 2$ dimer model ($H = 2JS_1 \cdot S_2$).[38] At this approximation, the g value is estimated at 1.92 and the coupling constant J/k_B at –1.4 K. The field dependence of the magnetization at 1.8 K has also been measured and is shown of Figure 9 (right). As in **6** and **8**, the magnetization at 1.8 K increases without saturation even at 7 Tesla at which it reaches 4.3 μ_B. Therefore, it would be necessary in this system as in **6** and **8** to apply a higher magnetic field in order to overcome the intermolecular antiferromagnetic interaction and to check the expected saturation value of the magnetization, here at 8 μ_B.

The ^1H NMR spectrum of **10** (Figure 10) shows strongly shifted signals for the protons of the phenyl thiolate ligands. Like in the ^1H NMR spectrum of $(Et_4N)_3[VFe_2S_4(SPh)_4]$[39] the signals for the *meta*-protons are found at lower energies (δ = 31.68 ppm), whereas the signals for the *ortho*- or *para*-protons are shifted to higher energies (δ = –23.71 and –29.50 ppm). The strong shifts are probably due to pseudocontact interactions. After ligand-to-metal charge transfer with antiparallel spin transfer, which gives rise to positive spin density on the sulfur atoms of the thiolate ligands, spin delocalization through the aromatic system – like in the equivalent radical – leads to positive spin density at the *ortho* and *para* positions.[40] Negative spin density at the nuclei of *ortho*- and *para*-hydrogen atoms and positive spin density at the nuclei of the *meta*-hydrogen atoms can be ascribed to spin-polarization effects.[41]

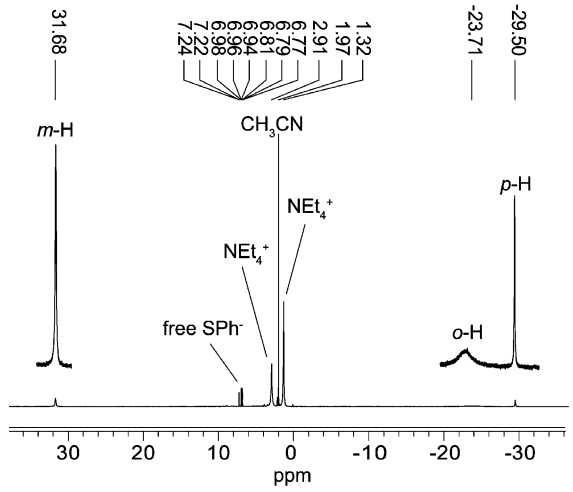

Figure 10. ^1H NMR spectrum of **11** in CD_3CN at 25 °C.

Treatment of **10** with 2 equiv. of $FeCl_2$ affords the ionic compound $(Et_4N)_3[Nb_2Fe_6S_8(SPh)_9]\cdot CH_3CN$ (**12**·CH_3CN). $(Et_4N)_3[Nb_2Fe_6Se_8(SePh)_9]\cdot CH_3CN$ (**13**·CH_3CN), the selenium derivative of **12**, was obtained by the reaction of $FeCl_2$, NaSe*t*Bu, Et_4NCl, $NbCl_5$ and NaSePh as shown in Scheme 3. Compounds **12** and **13** contain an $[Nb_2Fe_6E_8(EPh)_9]^{3-}$ anion [E = S (**12a**) (Figure 11), Se (**13a**)] which has an isostructural cluster core compared to the anions in $(Et_4N)_3[V_2Fe_6S_8(SEt)_9]\cdot CH_3CN$ and $(Et_4N)_3[Nb_2Fe_6S_8(SEt)_9]\cdot CH_3CN$[42] published by Holm et al.

Compounds **12a** and **13a** are built up by two distorted $[NbFe_3E_4]$ heterocubane units [E = S (**12a**), Se (**13a**)] (see Table 1) that are bridged by three μ_2-phenylthiolato (**12a**) and μ_2-phenylselenolato (**13a**) ligands, respectively. The $[NbFe_3]$ tetrahedra within the heterocubane core show deltahedral angles close to the ideal 60°, and the metal–metal distances are found within a narrow range (see Table 2). Each of the iron atoms in **12a** and **13a** is coordinated by three μ_3-chalcogenido and one terminal chalcog-

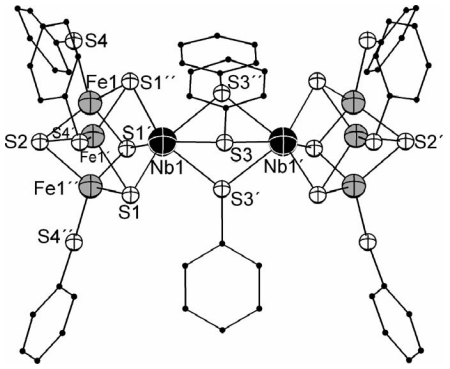

Figure 11. Molecular structure of **12a** in the solid state. Selected bond lengths [pm]: **12a**: Nb–μ_3-S 238.0(1), Nb–μ_2-S 264.2(1), Fe–μ_3-S 225.9(1)–227.6(1), Fe–S_t 225.0(1); **13a**: Nb–μ_3-Se 250.1(1), Nb–μ_2-Se 276.2(1), Fe– μ_3-Se 237.4(1)–239.7(1), Fe–Se_t 237.0(1).

enolato ligand that form a distorted tetrahedral coordination sphere (see Table 3). The niobium atoms are surrounded by three μ_3-chalcogenido and three μ_2-chalcogenolato ligands to afford a distorted octahedron.

The temperature dependence of the χT product at 0.1 Tesla is shown in Figure 12. Below 100 K, the system is in its singlet ground state. At temperatures above 100 K, excited states become thermally populated leading to a χT product of 0.85 cm^3K/mol at 300 K. This type of behavior has already been observed for $(Et_4N)_3[V_2Fe_6S_8(SEt)_9]\cdot CH_3CN$ and $(Et_4N)_3[Nb_2Fe_6S_8(SEt)_9]\cdot CH_3CN$.[41]

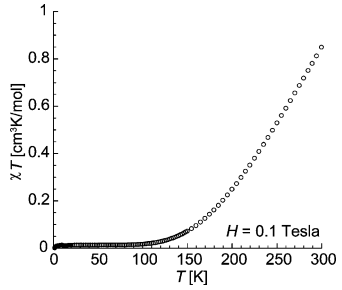

Figure 12. Magnetic measurement of **12**: χT vs. T plot at 0.1 Tesla.

The ^{1}H NMR spectrum of **12** (Figure 13) shows two sets of signals for the aromatic protons, one for the bridging (b) and one for the terminal (t) phenylthiolate groups. In each set of signals three signals for the *ortho*-, *meta*- und *para*-protons can be observed.

This means that the bridging and terminal ligands can be differentiated, and there is no fast exchange between them in solution. However, the ligands of one group are chemically equivalent in solution. The signals were assigned according to the following criteria: (1) *meta*- and *para*-protons show triplets, *ortho*-protons doublets; (2) the ratio of the integrations should be $o_b/m_b/p_b/o_t/m_t/p_t$ = 2:2:1:4:4:2; (3) the broadness of the signals increases in the sequence *para* < *meta* < *ortho*, because the distance to the paramagnetic centre increases in the same way.

The chemical shift of the *ortho*-, *meta*- und *para*-protons of the bridging ligands is similar to that of free phenylthiolate ions in a solution of NaSPh in acetonitrile,[43] because

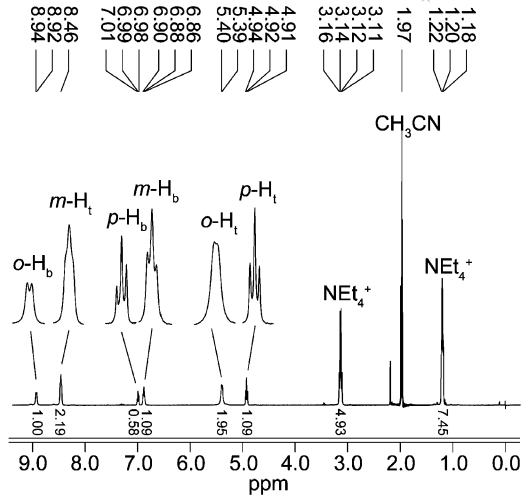

Figure 13. ^{1}H NMR spectrum of **12** in CD_3CN at 25 °C. Signal assignments are given (*o*, *m*, *p* = *ortho*, *meta*, *para*; t = terminal thiolate ligands, b = bridging thiolato ligands).

the shift increases in the sequence *meta* < *para* < *ortho*. The trend of the corresponding signals belonging to the protons of the terminal ligands is equivalent to that in **10** und **11** because the signals for the *para*- and *ortho*-protons are shifted to higher and for the *meta*-protons to lower energies. However, the effect in **13** is much weaker, and the signals are only weakly shifted. A similar trend can be observed in the ^{1}H NMR spectrum of $(n\mathrm{Bu}_4N)_3[Mo_2Fe_6S_8(SPh)_9]$.[44]

Conclusion

We synthesized new heterodimetallic chalcogen-bridged clusters containing niobium or tantalum in combination with the electron-rich transition metals iron, cobalt, or nickel. Thereby we were able to obtain a variety of structural arrangements of heterocubane molecules: neutral as well as ionic molecules containing a single heterocubane core and ionic molecules consisting of two triply bridged heterocubane units. The results of magnetic susceptibility measurements were helpful to obtain information on magnetic coupling within these clusters and magnetic ordering phenomena.

Experimental Section

General: All experiments were carried out under purified nitrogen. Solvents were dried with suitable drying agents and freshly distilled prior to use. $(Et_4N)_2[Fe(SPh)_4]$,[45] $[Li_3NbS_4]\cdot 2$tmeda[46] (tmeda = tetramethylethylenediamine), $Li_3[NbSe_4]$,[47] $S(SiMe_3)_2$, and $Se(SiMe_3)_2$[48] were prepared according to published methods. $NbCl_5$, $TaCl_5$, $TaBr_5$ $NiCl_2$, $NiBr_2$, $CoCl_2$, $FeCl_2$, PPh_3, dppm [bis(diphenylphosphanyl)methane] were purchased from Aldrich and used without further purification. The NMR spectra were recorded with a Bruker AC 250 spectrometer at 298 K. Chemical shifts are listed in parts per million (ppm) and reported relative to tetramethylsilane (^{1}H). Coupling constants are quoted in Hertz (Hz). Residual solvent peaks were used as internal standards (δ =1.97 ppm for

CH_3CN). All infrared spectra were recorded as KBr pellets with a Bruker XIFS 28 spectrometer, and the results are reported in cm^{-1}. The ESI mass spectra were obtained with an Ionspec Ultima FT-ICR spectrometer with an Analytica electrospray source and a 7.0 Tesla magnet. The elemental analyses were performed with a Vario EL analysing automate of the company Elementar-Analysensysteme. The magnetic susceptibility measurements were obtained using a Quantum Design Squid magnetometer MPMS-XL that works between 1.8 and 400 K for dc applied fields ranging from –7 to 7 Tesla. The absorption spectra were recorded with a Perkin–Elmer UV/Vis/NIR spectrometer (Lambda 900). The reported procedures are optimised with respect to the resulting compounds. In some cases we observed the precipitation of amorphous powder during the reaction. The given yields are based on the weight of the isolated crystalline substances.

$[Nb_2Ni_2S_4Cl_4(PPh_3)_2(CH_3CN)_2]\cdot 2CH_3CN$ (1·2CH_3CN): 269 mg (0.41 mmol) of $[NiCl_2(PPh_3)_2]$ was dissolved in 10 mL of acetonitrile and combined with a solution of 166 mg (0.62 mmol) of $NbCl_5$ in 5 mL of acetonitrile. Then 0.26 mL (220 mg, 1.23 mmol) of $S(SiMe_3)_2$ was added to the reaction mixture which was stirred at 80 °C overnight. A resulting insoluble black solid was removed from the reaction mixture by filtration, and the dark green filtrate was kept at –20 °C for two weeks before **1** was obtained in the form of black needle-shaped crystals. The product crystallized together with a small amount of unidentified by-product, and efforts to recrystallize it resulted in decomposition of **1**. This is the reason why we were not able to isolate a completely pure product (yield: approximately 60% based on nickel). IR (KBr): $\tilde{\nu}$ = 426 (m), 518 (vs), 690 (vs), 741 (s), 870 (w), 996 (w), 1094 (s), 1307 (w), 1433 (vs), 1478 (m), 1583 (w), 3045 (w) cm^{-1}. UV/Vis/NIR (CH_3CN): λ (lg ε) = 609 (3.200), 508 (3.168), 312 (6.817), 254 (7.345) nm.

$[Nb_2Ni_2Se_4Cl_4(PPh_3)_2(CH_3CN)_2]\cdot 2CH_3CN$ (2·2CH_3CN): 350 mg (0.53 mmol) of $[NiCl_2(PPh_3)_2]$ was dissolved in 10 mL of acetonitrile and combined with a stirred solution of 216 mg (0.80 mmol) of $NbCl_5$ in 5 mL of acetonitrile. Then 0.40 mL (360 mg, 1.42 mmol) of $Se(SiMe_3)_2$ was added to the reaction mixture. After 2 min of stirring, a colour change from light green to dark brown was observed. To remove the insoluble black solid the reaction mixture was filtered, and the resulting greenish-brown filtrate was stored at –20 °C for two weeks before **2** was obtained in the form of black needle-shaped crystals. The product crystallized together with a small amount of unidentified by-product, and efforts to recrystallize it resulted in decomposition of **2**. This is the reason why we were not able to isolate a completely pure product (yield: approximately 30% based on nickel). IR (KBr): $\tilde{\nu}$ = 427 (vw), 449 (vw), 504 (s), 510 (s), 561 (vs), 617 (vw), 690 (vs), 710 (m), 744 (m), 750 (m), 800 (vw), 996 (w), 1025 (w), 1067 (vw), 1095 (s), 1156 (vw), 1179 (vw), 1259 (w), 1304 (w), 1433 (vs), 1478 (m), 3051 (w) cm^{-1}. UV/Vis/NIR (CH_3CN): λ (lgε) = 608 (3.314), 504 (3.377), 266 (4.595), 215 (5.380) nm.

$[Ta_2Ni_2S_4Br_4(PPh_3)_2(CH_3CN)_2]\cdot 2.5CH_3CN$ (3·2.5CH_3CN): A suspension of 252 mg (0.43 mmol) of $TaBr_5$ in 20 mL of acetonitrile was combined with 350 mg (0.47 mmol) of $[NiBr_2(PPh_3)_2]$. Then, 0.2 mL (1.00 mmol) of $S(SiMe_3)_2$ was added to the reaction mixture. After stirring at 80 °C for 1 h, the reaction mixture was filtered to remove a black insoluble solid. The red-brown filtrate was stored at room temperature for 2 h before black needle-shaped crystals of **3** formed (yield: 40% based on nickel). $C_{45}H_{43.5}Br_4N_{4.5}Ni_2P_2S_4Ta_2$ (1636.48): calcd. C 31.09, H 2.35, N 1.81; found C 31.73, H 2.65, N 2.30. IR (KBr): $\tilde{\nu}$ = 403 (vw), 427 (vw), 493 (w), 509 (m), 521 (vs), 692 (vs), 706 (w), 743 (m), 801 (w), 997 (w), 1024 (w), 1095 (s), 1157 (vw), 1180 (vw), 1260 (w), 1435 (vs), 1478 (m), 1582 (w), 2958 (vw), 3047 (vw), 3426 (br. w) cm^{-1}. UV/Vis/NIR (CH_3CN): λ (lgε) = 729 (2.090), 472 (2.758), 379 (3.132), 288 (3.478), 250 (3.630), 201 (4.853) nm.

$[Ta_2Ni_2Se_4Br_4(PPh_3)_2(CH_3CN)_2]\cdot 2.5CH_3CN$ (4·2.5CH_3CN): 170 mg (0.29 mmol) of $TaBr_5$ was added to a suspension of 225 mg (0.30 mmol) of $[Ni(PPh_3)_2Br_2]$ in acetonitrile. After adding 0.08 mL (0.4 mmol) of $Se(SiMe_3)_2$ to the reaction mixture, it was stirred at 80 °C for 30 min. The black reaction solution was left at room temperature for 5 d before black, needle-shaped crystals of **4** formed (yield: 10% based on nickel). IR (KBr): $\tilde{\nu}$ = 423 (w), 492 (m), 508 (m), 520 (vs), 561 (w), 616 (vw), 690 (vs), 701 (m), 743 (m), 798 (w), 638 (vw), 997 (w), 1025 (w), 1068 (w), 1094 (s), 1156 (w), 1180 (w), 1260 (w), 1307 (vw), 1382 (vw), 1433 (vs), 1478 (m), 1570 (w), 1583 (w), 1629 (vw), 2278 (vw), 2309 (vw), 3048 (w) cm^{-1}.

$[Ni_3S_2(PMe_3)_6][Ta_3NiS_4(PMe_3)_4Cl_6]_2$ (5): A suspension of 102 mg (0.79 mmol) of $NiCl_2$ in 5 mL of acetonitrile was combined with a solution of 272 mg (0.76 mmol) of $TaCl_5$ in 5 mL of acetonitrile. Addition of 0.30 mL (3.00 mmol) of PMe_3 led to a deep red solution. After 0.4 mL (2.00 mmol) of $S(SiMe_3)_2$ was added to the reaction mixture, it was stirred for 3 h, and a colour change to red brown was observed. After six weeks at room temperature, brown crystals of **5** formed (yield: 10% based on nickel).

$[Fe(dppm)_2(CH_3CN)_2][NbFe_3S_4Cl_3(dppm)(CH_3CN)]_2\cdot 4CH_3CN\cdot 2CH_2Cl_2$ (6·4CH_3CN·2CH_2Cl_2): 135 mg (1.07 mmol) of $FeCl_2$ was dissolved in 10 mL of acetonitrile to form a pale yellow solution which was then treated with a solution of 700 mg (1.07 mmol) of dppm in 5 mL of dichloromethane. A solution of 76 mg (0.28 mmol) of $NbCl_5$ in 1 mL of acetonitrile was added, and 0.22 mL (191 mg, 1.07 mmol) of $S(SiMe_3)_2$ was transferred to the reaction mixture. After storing the dark brown solution at room temperature for one week, **6** precipitated in the form of very small, brown, plate-like crystals (yield: 16% based on iron. $C_{108}H_{100}Cl_6Fe_7N_4Nb_2P_8S_8$ (2747.79): calcd. C 47.21, H 3.67, N 2.04; found C 47.41, H 3.54, N 1.91. IR (KBr): $\tilde{\nu}$ = 498 (m), 476 (m), 474 (m), 507 (s), 511 (m), 694 (vs), 737 (s), 798 (m), 998 (m), 1022 (m), 1094 (vs), 1156 (w), 1185 (w), 1260 (m), 1308 (w), 1354 (w), 1434 (vs), 1482 (m), 1571 (w), 1582 (w), 2261 (vw), 2094 (w), 2959 (w), 3048 (w) cm^{-1}. UV/Vis/NIR (CH_3CN): λ (lgε) = 248 (4.820), 213 (4.886) nm.

$[Fe(dppm)_2(CH_3CN)_2][TaFe_3S_4Cl_3(dppm)(CH_3CN)]_2\cdot 4CH_3CN\cdot 2CH_2Cl_2$ (7·4CH_3CN·2CH_2Cl_2): 51 mg (0.40 mmol) of $FeCl_2$ was dissolved in 5 mL of acetonitrile to form a pale yellow solution. To the latter a solution of 262 mg (0.68 mmol) of dppm in 2.8 mL of dichloromethane was added. The colour of the reaction mixture changed to red. By the addition of 47 mg (0.13 mmol) of $TaCl_5$, dissolved in 1.9 mL of acetonitrile, the colour changed to orange-red. Finally, 0.84 mL (0.4 mmol) of $S(SiMe_3)_2$ was added to the stirred reaction mixture which within a few seconds changed its colour to deep red and then to dark brown. After storing the solution at room temperature for 5 d, black needle-shaped crystals of **7** were obtained (yield: 10% based on iron). $C_{108}H_{100}Cl_6Fe_7N_4P_8S_8Ta_2$ (2923.87): calcd. C 44.37, H 3.45, N 1.92; found C 44.27, H 3.44, N 1.15. IR (KBr): $\tilde{\nu}$ = 400 (s), 475 (s), 501 (s), 520 (s), 689 (s), 721 (m), 735 (s), 791 (w), 835 (vw), 905 (vw), 998 (m), 1025 (w), 1094 (m), 1158 (w), 1185 (w), 1262 (w), 1306 (w), 1332 (w), 1339 (w), 1354 (w), 1435 (vs), 1481 (m), 1571 (w), 1583 (w), 3047 (br. w), 3455 (br. w) cm^{-1}. UV/Vis/NIR (CH_3CN): λ (lgε) = 251 (5.10), 466 (3.80), 629 (3.33) nm.

$[Fe(dppmSe)_2Cl][TaFe_3Se_4Cl_3(dppm)(CH_3CN)]\cdot CH_2Cl_2$ (8·CH_2Cl_2): 44 mg (0.12 mmol) of $TaCl_5$ was dissolved in 10 mL of acetonitrile and combined with a suspension of 100 mg (0.04 mmol) of $[Fe_8Se_9(dppm)_3]$[28] in 5 mL of dichloromethane. After stirring the

reaction mixture at 80 °C for 2 h, it was filtered to remove an insoluble solid. The dark black filtrate was stored at 0 °C for six weeks before black cube-shaped crystals of **8** formed (yield: 15% based on iron). $C_{78}H_{69}Cl_4Fe_4NP_6Se_6Ta$ (2226.16): calcd. C 42.08, H 3.12, N 0.63; found C 41.28, H 3.09, N 1.27. IR (KBr): $\tilde{\nu}$ = 423 (m), 473 (m), 505 (s), 521 (s), 689 (vs), 720 (s), 737 (vs), 774 (m), 998 (m), 1024 (w), 1068 (w), 1094 (s), 1149 (w), 1185 (w), 1260 (w), 1308, 1331 (w), 1353 (w), 1435 (vs), 1481 (m), 1574 (w), 1584 (w), 2879 (vw), 2931 (vw), 3050 (w), 3064 (w), 3485 (br.·vw) cm^{-1}. UV/Vis/NIR (CH_3CN): λ ($lg\varepsilon$) = 243 (4.83), 514 (3.35), 727 (3.07) nm.

$[NbCo_3Se_4(PPh_3)_3(CH_3CN)_3][CoCl_3(PPh_3)]\cdot 4CH_3CN$ (9·4CH_3CN): 87 mg (0.32 mmol) of $NbCl_5$ and 912 mg (1.288 mmol) of $[CoCl_2(PPh_3)_2]$ were dissolved in 40 mL of acetonitrile. Then, 0.32 mL (288 mg, 1.288 mmol) of $Se(SiMe_3)_2$ was added to the stirred reaction mixture leading to a colour change from greenish-blue to black. After storing the solution at 0 °C for 2 d, blue crystals of $[CoCl_2(PPh_3)_2]$ formed. The solution was stored at –20 °C for another 7 d before **9** crystallised in the form of small needle-shaped black crystals (yield: 11% based on cobalt). IR (KBr): $\tilde{\nu}$ = 516 (s), 564 (w), 668 (s), 692 (vs), 725 (w), 1095 (m), 1244 (br. m), 1419 (s), 1662 (w, br), 2867 (vw), 2933 (vw), 3045 (w) cm^{-1}.

$(Et_4N)_3[NbFe_2S_4(SPh)_4]$ (10): 571 mg (0.76 mmol) of $(Et_4N)_2[Fe(SPh)_4]$ was dissolved in 10 mL of acetonitrile and added to 180 mg (0.38 mmol) of Li_3NbS_4·2tmeda. A dark red solution was formed, and after storing it at 0 °C for 3 d, red crystals of **10** formed (yield: 11% based on iron). $C_{48}H_{80}Fe_2N_3NbS_8$ (1160.31): calcd. C 49.69, H 6.95, N 3.62; found C 49.58, H 6.79, N 3.72. ^{1}H NMR (400.1 MHz, 25 °C, CD_3CN): δ = –29.472 (br., *p-H*, SPh), –23.673 (br., *o-H*, SPh), 1.309 [br., 36 H, $N(CH_2CH_3)_4$], 1.967 (q, CH_3CN), 2.919 [br., $N(CH_2CH_3)_4$], 6.820 (t, *p-H*, free SPh^-), 6.986 (t, *m-H*, free SPh^-), 7.251 (d, *o-H*, free SPh^-), 31.669 (br., t, *m-H*, SPh) ppm. IR (KBr): $\tilde{\nu}$ = 437 (m), 473 (w), 692 (s), 744 (vs), 781 (w), 888 (vw), 999 (w), 1023 (m), 1083 (s), 1169 (m), 1260 (w), 1385 (m), 1432 (m), 1472 (vs), 1574 (vs), 2968 (w), 3041 (vw) cm^{-1}. UV/Vis/NIR (CH_3CN): λ ($lg\varepsilon$) = 288 (4.133), 321 (4.383), 442 (4.522) nm. ESI-MS (CHCN): *m*/*z* (%) = 1291 (100) $\{(Et_4N)_4[NbFe_2S_4(SPh)_4]\}^+$.

$(Et_4N)_3[NbFe_2Se_4(SPh)_4]$ (11): 753 mg (1.00 mmol) of $(Et_4N)_2[Fe(SPh)_4]$ was dissolved in 10 mL of acetonitrile and added to 251 mg (0.50 mmol) of Li_3NbSe_4. A dark red solution formed, and after storing it at 0 °C for 4 d, red crystals of **11** formed (yield: 10% based on iron). $C_{48}H_{80}Fe_2N_3NbS_4Se_4$ (1347.89): calcd. C 42.77, H 5.98, N 3.12; found C 42.86, H 6.04, N 3.19. ^{1}H NMR (400.1 MHz, 25 °C, CD_3CN): δ = –30.770 (br., *p-H*, SPh), –24.653 (br., *o-H*, SPh), –23.930 (br., *p-H*, SPh), –16.123 (br., *o-H*, SPh), 1.290 [br., 36 H, $N(CH_2CH_3)_4$], 1.967 (q, CH_3CN), 3.121 [br., 36 H, $N(CH_2CH_3)_4$], 6.755 (t, *p-H*, free SPh^-), 6.928 (t, *m-H*, free SPh^-), 7.236 (d, *o-H*, free SPh^-), 22.668 (br. t, *m-H*, SPh), 32.199 (br. t, *m-H*, SPh) ppm. IR (KBr): $\tilde{\nu}$ = 427 (w), 473 (w), 690 (m), 743 (s), 777 (w), 787 (w), 886 (vw), 999 (w), 1021 (m), 1066 (w), 1085 (m), 1170 (m), 1260 (w), 1389 (m), 1431 (m), 1472 (vs), 1478 (s), 1574 (s), 1630 (vw), 2848 (vw), 2915 (w), 2969 (w), 3038 (vw), 3432 (br. w) cm^{-1}. UV/Vis/NIR (CH_3CN): λ ($lg\varepsilon$) = 555 (6.515), 474 (6.930), 432 (6.970), 291 (7.428), 264 (7.524) nm.

$(Et_4N)_3[Nb_2Fe_6S_8(SPh)_9]\cdot CH_3CN$ (12·CH_3CN): 278 mg (0.37 mmol) of $(Et_4N)_2[Fe(SPh)_4]$ was dissolved in 10 mL of acetonitrile and combined with 175 mg (0.37 mmol) of Li_3NbS_4·2tmeda to form **10**. To the reaction mixture a solution of 47 mg (0.37 mmol) of $FeCl_2$ in 5 mL of acetonitrile was added. After storing the solution at 0 °C for 3 d, black crystals of **12** formed (yield: 26% based on iron). ^{1}H NMR (400.1 MHz, 25 °C, CD_3CN, 298 K): δ = 1.20 [t, *J* = 8 Hz, 36 H, $N(CH_2CH_3)$], 1.97 (m, CH_3CN), 3.13 [q, *J* = 8 Hz, 24 H, $N(CH_2CH_3)$], 4.92 (t, *J* = 5 Hz, 6 H, *p*-H_t), 5.40 (d, *J* = 5 Hz, 12 H, *o*-H_t), 6.88 (t, *J* = 7 Hz, 6 H, *m*-H_b), 6.99 (t, *J* = 7 Hz, 3 H, *p*-H_b), 8.46 (br. t, 12 H, *m*-H_t), 8.93 (d, *J* = 7 Hz, 6 H, *o*-H_b) ppm. IR (KBr): $\tilde{\nu}$ = 410 (w), 473 (w), 690 (s), 741 (s), 782 (w), 998 (w), 1021 (m), 1066 (w), 1083 (m), 1170 (w), 1179 (vw), 1261 (vw), 1366 (w), 1391 (m), 1433 (s), 1456 (m), 1472 (vs), 1575 (s), 2978 (w), 3047 (w), 3456 (br. w) cm^{-1}. UV/Vis/NIR (CH_3CN): λ ($lg\varepsilon$) = 409 (7.469), 339 (7.565), 238 (7.933) nm. ESI-MS (CHCN): *m*/*z* (%) = 2282 (100) $\{(Et_4N)_4[Nb_2Fe_6S_8(SPh)_9]\}^+$.

$(Et_4N)_3[Nb_2Fe_6Se_8(SePh)_9]\cdot CH_3CN$ (13·CH_3CN): A solution of 135 mg (0.5 mmol) of $NbCl_5$ in 3 mL of acetonitrile was added to a suspension of 190 mg (1.51 mmol) of $FeCl_2$, 477 mg (3.00 mmol) of NaSe*t*Bu and 132 mg (0.80 mmol) of Et_4NCl in 20 mL of acetonitrile. Then, 0.72 mL (3.00 mmol) of $PhSeSiMe_3$ was transferred to the reaction mixture which was stirred overnight. The reaction mixture was filtered to remove insoluble brown solid, and the filtrate was layered with 5 mL of diethyl ether. After three weeks at room temperature, black crystals of **13** formed (yield: 10% based on iron).

Acknowledgments

The authors thank Dr. Ralf Burgert (Univerität Karlsruhe) for recording the mass spectra. The Centrum für Funktionelle Nanostrukturen (CFN), the Deutsche Forschungsgemeinschaft, the Université Bordeaux 1, the Centre National de la Recherché Scientifique (CNRS), and the Région Aquitaine are acknowledged for financial support.

[1] E. I. Stiefel, K. Matsumoto, *Transition Metal Sulfur Chemistry*, ACS Symposium Series, Honululu, Hawaii, **1995**.
[2] V. P. Fedin, J. Czyzniewska, R. Prins, T. Weber, *Appl. Catal. A* **2001**, *213*, 123.
[3] T. Weber, R. Prins, R. A. van Santen, *Transition Metal Sulfides – Chemistry and Catalysis*, Kluwer, Dordrecht, **1998**.
[4] E. Wolff, J. M. Berg, K. O. Hodgson, R. B. Frankel, R. H. Holm, *J. Chem. Soc., Chem. Commun.* **1979**, *101*, 4140.
[5] Q.-F. Zhang, Y.-N. Xiong, T.-S. Lai, W. Ji, X.-Q. Xin, *J. Phys. Chem. B* **2000**, *104*, 3446.
[6] M. Feliz, J. M. Garriga, R. Llusar, S. Uriel, M. G. Humphrey, N. T. Lucas, M. Samoc, B. Luther-Davis, *Inorg. Chem.* **2001**, *40*, 6132.
[7] S.-B. Yu, A. B. Watson, *Chem. Rev.* **1999**, *99*, 2353.
[8] S.-B. Yu, M. Droege, B. Segal, S. H. Kim, T. Sanderson, A. D. Watson, *Inorg. Chem.* **2000**, *39*, 1325.
[9] B. Hales, E. Case, J. Morningstar, M. Dzeda, L. Mauterer, *Biochemistry* **1986**, *25*, 7251.
[10] A. Müller, J. Schimanski, H. Bögge, *Z. Anorg. Allg. Chem.* **1987**, *544*, 107.
[11] a) A. Lorenz, D. Fenske, *Angew. Chem.* **2001**, *113*, 4537; *Angew. Chem. Int. Ed.* **2001**, *40*, 4402; b) R. Pätow, D. Fenske, *Z. Anorg. Allg. Chem.* **2002**, *628*, 1279.
[12] S. Ciurli, R. H. Holm, *Inorg. Chem.* **1989**, *28*, 1685.
[13] G. Christou, C. D. Garner, T. J. King, C. E. Johnson, J. D. Rush, *J. Chem. Soc., Chem. Commun.* **1979**, 503.
[14] M. Koutmos, D. Coucouvanis, *Angew. Chem.* **2004**, *116*, 5133; *Angew. Chem. Int. Ed.* **2004**, *43*, 5023.
[15] M. Koutmos, D. Coucouvanis, *Inorg. Chem.* **2004**, *43*, 6508.
[16] R. Pätow, I. Isaac, D. Fenske, *Z. Anorg. Allg. Chem.* **2003**, *629*, 1437.
[17] W. Cen, S. C. Lee, J. Li, F. M. MacDonnell, R. H. Holm, *J. Am. Chem. Soc.* **1993**, *115*, 9515.
[18] G. M. Sheldrick, *SHELXTL-97*, University of Göttingen, **1997**.
[19] G. M. Sheldrick, *SHELXTL-97*, University of Göttingen, **1997**.

[20] R. Pätow, D. Fenske, *Z. Anorg. Allg. Chem.* **2002**, *628*, 1279.
[21] R. A. Jones, B. R. Whittleesey, *Inorg. Chem.* **1986**, *25*, 852.
[22] R. A. Jones, A. L. Stuart, J. L. Atwood, W. E. Hunter, *Organometallics* **1983**, *2*, 874.
[23] K. Herbst, P. Zanello, M. Corsini, N. D'Amelio, L. Dahlenburg, M. Brorson, *Inorg. Chem.* **2003**, *42*, 974.
[24] T. Shibahara, M. Yamasaki, H. Akashi, T. Katayama, *Inorg. Chem.* **1991**, *30*, 2693.
[25] C. A. Ghilardi, S. Midollini, L. Sacconi, *Inorg. Chim. Acta* **1978**, *31*, L431.
[26] D. Fenske, H. Fleischer, H. Krautscheid, J. Magull, *Z. Naturforsch., B: Chem. Sci.* **1990**, *45*, 127.
[27] H. Vahrenkamp, V. A. Uchtman, L. F. Dahl, *J. Am. Chem. Soc.* **1968**, *90*, 3272.
[28] I. Issac, unpublished results.
[29] J. A. Kovacs, R. H. Holm, *Inorg. Chem.* **1987**, *26*, 207.
[30] K. D. Demadis, D. Coucouvanis, *Inorg. Chem.* **1995**, *34*, 436.
[31] J. Han, M. Huang, D. Coucouvanis, *Polyhedron* **2002**, *21*, 2523.
[32] L. M. D. R. S. Martins, M. T. Duarte, A. M. Galvao, C. Resende, A. J. L. Pombeiro, R. A. Henderson, D. J. Evans, *J. Chem. Soc., Dalton Trans.* **1998**, 3311.
[33] J. E. Barclay, A. Hills, D. L. Hughes, G. J. Leigh, *J. Chem. Soc., Dalton Trans.* **1988**, 2871.
[34] L. Sacconi, M. Di Vaira, *Inorg. Chem.* **1978**, *17*, 810.
[35] a) R. E. Palermo, R. Singh, J. K. Bashkin, R. H. Holm, *J. Am. Chem. Soc.* **1984**, *106*, 2600; b) S. M. Malinak, A. Simeonov, P. E. Moisier, C. E. McKenna, D. Coucouvanis, *J. Am. Chem. Soc.* **1997**, *119*, 1662.
[36] K. D. Demadis, D. Coucouvanis, *Inorg. Chem.* **1995**, *34*, 436.
[37] Y. Do, E. D. Simhon, R. H. Holm, *Inorg. Chem.* **1985**, *24*, 4635.
[38] O'Connor, *Prog. Inorg. Chem.* **1982**, *29*, 203.
[39] Y. Do, E. D. Simhon, R. H. Holm, *Inorg. Chem.* **1985**, *24*, 4635.
[40] R. H. Holm, W. D. Phillips, B. A. Averill, J. J. Mayerle, T. Herskovitz, *J. Am. Chem. Soc.* **1974**, *96*, 2109–2117.
[41] G. N. La Mar, W. DeW. Horrocks Jr., R. H. Holm, *NMR of Paramagnetic Molecules, Principles and Applications*, Academic Press, New York, **1973**.
[42] W. Cen, S. C. Lee, J. Li, F. M. MacDonnell, R. H. Holm, *J. Am. Chem. Soc.* **1993**, *115*, 9515.
[43] B. Bechlars, Dissertation, Universität Karlsruhe, **2007**.
[44] G. Christou, C. D. Garner, *J. Chem. Soc., Dalton Trans.* **1980**, 2354.
[45] K. S. Hagen, J. G. Reynolds, R. H. Holm, *J. Am. Chem. Soc.* **1981**, *103*, 4054.
[46] a) S. C. Lee, R. H. Holm, *J. Am. Chem. Soc.* **1990**, *112*, 9654; b) S. C. Lee, J. G. Li, J. C. Mitchell, R. H. Holm, *Inorg. Chem.* **1992**, *31*, 4333.
[47] R. Feuerhake, Dissertation, Universität Karlsruhe, **2004**.
[48] H. Schmid, H. Ruf, *Z. Anorg. Allg. Chem.* **1963**, *321*, 270.

Received: October 25, 2007
Published Online: February 18, 2008

